Heat Transfer Enhancement by Nanofluid Coupling with Surfactant in Overcoming Particle Agglomeration for Microchannel Heat Sinks

Mohamad Nur Hidayat Mat[1*] and R. Saidur[2,3]

[1]School of Mechanical Engineering, Faculty of Engineering, Universiti Teknologi Malaysia,

81310 UTM Johor Bahru, Malaysia

[2]Research Centre for Nano-Materials and Energy Technology (RCNMET), School of

Engineering and Technology, Sunway University, No. 5, Jalan Universiti, Bandar Sunway,

Petaling Jaya, 47500 Selangor Darul Ehsan, Malaysia

School of Engineering, Lancaster University, Lancaster LA1 4YW, UK.

*Corresponding author: mn.hidayat@utm.my; Tel.: (+60) 133110073

Abstract

The characteristic effect of nanoparticles, Boron Nitride nanotubes (BNNTs) in the nanofluid with and without surfactant, was investigated using numerical CFD. A simplified microchannel heat sink model was created and discretized for numerical analysis. The numerical prediction was validated with previous experiment data for promising numerical agreement. Then, the effect of different Triton X-100 surfactant volume fractions and nanotube mass fractions in the base fluid were carried out on thermal and hydraulic performance. The significant finding revealed that the thermal resistance was reduced by as much as 90 % compared to pure water with a surfactant concentration of 0.35 *vol.* % and adding 0.02 *wt.* % at the Reynold number (*Re*) of 400. However, the Nusselt number (*Nu*) increased twice from the pure water with an

additional surfactant of 0.35 *vol.* % after the *Re* of 400. Despite improving the thermal performance, the pressure drop seems to be a drawback for the nanotube with surfactant implementation. The outcome of the present study provided a better understanding of the nanofluid flow with surfactant effect in the nanofluid in the microchannel heat sink so that better design decisions can be made for the improvement of this application for different needs.

Keywords

Microchannel heat sink; numerical; nanofluid; nanotube; surfactant.

Nomenclature

c_p	specific heat, $\text{J}\cdot\text{kg}^{-1}\cdot\text{K}^{-1}$
$c_{p_{bf}}$	specific heat of base fluid, $\text{J}\cdot\text{kg}^{-1}\cdot\text{K}^{-1}$
D	diameter, m
h	heat transfer coefficient, $\text{W}\cdot\text{m}^{-2}\cdot\text{K}^{-1}$
k	thermal conductivity, $\text{W}\cdot\text{m}^{-1}\cdot\text{K}^{-1}$
k_{bf}	thermal conductivity of the base fluid, $\text{W}\cdot\text{m}^{-1}\cdot\text{K}^{-1}$
$k_{Brownian}$	Brownian, $\text{W}\cdot\text{m}^{-1}\cdot\text{K}^{-1}$
k_{eff}	effective thermal conductivity of Brownian
k_{static}	static thermal conductivity, $\text{W}\cdot\text{m}^{-1}\cdot\text{K}^{-1}$
Nu	Nusselt number
P	pressure, Pa
q	heat flux, $\text{W}\cdot\text{m}^{-2}$

R	thermal resistance, $\text{m}^2 \cdot \text{K} \cdot \text{W}^{-1}$
Re	Reynolds number
T	temperature, K
v	velocity, $\text{m} \cdot \text{s}^{-1}$
$\dot{W}$	pumping power, W
μ	dynamic viscosity, Pa·s
μ_{eff}	effective dynamic viscosity, Pa·s
μ_{static}	static dynamic viscosity, Pa·s
$\mu_{Brownian}$	Brownian dynamic viscosity, Pa·s
μ_{bf}	dynamic viscosity of the base fluid, Pa·s
ρ	density, $\text{kg} \cdot \text{m}^{-3}$
ρ_{bf}	density of the base fluid, $\text{kg} \cdot \text{m}^{-3}$
vol	nanoparticle volume fraction, %

Subscripts

α	channel aspect ratio
β	wall width ratio
W	heat sink width, (cm)
L	heat sink length, (cm)
t	substrate thickness, (mm)
H_c	channel height, (mm)

1.0   Introduction

A microchannel heat sink (MCHS) is an advanced cooling technique that removes excess heat from electrical and electronic device components through a cooling medium (Zhou et al., 2020). The cooling medium is made of distilled water as a heat transfer carrier. Due to the fourth industrialization, this standalone distilled water in MCHS has its limitation of dissipating a large amount of heat flux from a small area (Drummond et al., 2018; Monavari, Jamaati, & Bahiraei, 2021). Therefore, nanoparticles have been added to assist the heat transfer process and are still a hot spot in recent years.

So far, several techniques have been proposed to improve the performance of MCHS, such as using various cooling fluids (Bahiraei, Mazaheri, & Daneshyar, 2021; Chuan, Wang, Wang, & Yan, 2015; Xia et al., 2015), different rib channels (Ghani et al., 2017; Japar, Sidik, & Mat, 2018), introduce channel porosity (Gong, Li, Bai, & Xu, 2018), adding several fins (Fisher & Torrance, 2001; Knight, Hall, Goodling, & Jaeger, 1992; Wei & Joshi, 2003), and apply different channel geometries (Alhamid, Nasruddin, Susanto, Vickary, & Budiyanto, 2019; Ardiansyah, Orlando, Rahman, & Prihantini, 2019; Bahiraei, Heshmatian, Goodarzi, & Moayedi, 2019; Bahiraei & Monavari, 2020; Monavari et al., 2021; Weisberg, Bau, & Zemel, 1992). Among those techniques, adding nanoparticles to the base fluid is straightforward but efficient. This approach is easy, cost-effective, and simple to install compared to fabricating a new geometry. However, a substantial amount of nanoparticles would cause particle instability resulting in particle agglomeration in the channel (Heidarshenas, Azizi, Peyghambarzadeh, & Sayyahi, 2021).

Several methods have been used to attain the stability of the nanotubes. These methods include sonification, high shear, high-pressure homogenization, controlling pH value, surfactant, surface modification technique, and ball milling (Dey, Kumar, & Samantaray, 2017). Adding

surfactant to the nanofluid is one of the economical and most straightforward methods to improve the stability of the nanotubes. The surfactant may be anionic, cationic, or anionic, such as Sodium dodecyl sulfate (SDS) and polyvinyl pyrrolidone (PVP). These surfactants act as a stabilizing agent for the nanoparticles in the nanofluid by reducing the interfacial tension between nanoparticles (Babu, Kumar, & Rao, 2017). Based on the effectiveness, a study was conducted using 0.01% surfactant with TiO2 nanofluids, and the thermal conductivity increased by 33% when using 5% nanotubes (Murshed, Leong, & Yang, 2005). An investigation on the dispersion stability of Al_2O_3 nanotube in the nanofluid with and without surfactant was done. This study discovered that the nanoparticles' dispersion increased with the surfactant concentration increase in the nanofluid (Li et al., 2008). Besides, an investigation of cupper-ethylene glycol nanofluid with PVP surfactant concluded that the stability of the nanotubes could be improved by adding the surfactant (Yu, Xie, Chen, & Li, 2010).

Triton X-100 has been used as a surfactant for heat transfer improvement in the nanofluid. An experimental study reported that TX-100 at 30 °C improved MCHS's thermal capability even without nanoparticles (Shamsuddin, Estellé, Navas, Mohd-Ghazali, & Mohamad, 2021). An experimental study of thermosyphon heat pipe uses TX-100 as a surfactant. They reported combining TX-100 with Boron Nitride Nanoparticles (BNNTs) in nanofluid resulting in lower thermal resistance and higher thermal efficiency of the heat pipe system (Ghorabaee, Emami, & Shafahi, 2020). Another finding reported that the heat pipe efficiency could be increased by up to 20.9 % by adding approximately 2% of TX-100's concentration. The application of TX-100 also has been reported to be used in a solar collector. The result described that additional TX-100 in the nanofluid that contains TiO_2 nanotubes provided excellent performance than water (Kiliç, Menlik, & Sözen, 2018). In addition, Triton TX-100 strongly

5

influenced the suspension stability and absorption characteristic of sunlight for multi-walled carbon nanotubes in nanofluid to enhance solar thermal absorption (Choi, Jang, & Kedzierski, 2018). Despite the benefits of the surfactants, significant limitations and adverse effects of surfactants have been recorded so far, such as foam foaming at high temperatures. This effect may degrade the thermal performance of the fluid flow (Dey et al., 2017). Therefore, to our knowledge, no work has been reported on the combined effect of Triton X-100 as a surfactant with the nanoparticle BNNT for Microchannel heat sink using the numerical CFD approach. Thus, this research is focused on closing this gap.

In this study, numerical CFD was conducted to investigate the effect of adding TX-100 surfactant on Boron Nitride nanoparticles. This approach can clarify the complex flow and heat transfer patterns inside MCHS with much more detail and reduce cost. To clearly understand the effect of this additional surfactant, three (3) different fluids were created: distilled water alone, TX-100 mixing with distilled water, and TX-100 mixing with BNNT nanoparticle in distilled water. These categories of fluid were simulated against Reynold's number and temperature. The characteristic effect of heat transfer in terms of thermal resistance, Nusselt number, and pressure drop presented in contour plots would be a novelty for this research.

The paper is organized as follows, the definition of different fluids used is presented in section 2.0, and geometrical parameters are described in the problem statement. The governing equation described the equation used in the CFD study is shown in section 2.0, and the definition of performance indicators is in section 2.4. Validation study through grid-independent tests as detailed in section 2.8. Finally, the result and discussion in section 3.0 and the conclusion appeared in the last section.

2.0   Methodology

2.1   Concentration of fluid

The heat transfer effect and the pressure drop of a microchannel heat sink were investigated at different concentrations of Triton TX-100 surfactant ranging from 0.005 *vol.* % to 0.035 *vol.* % with an increment of 0.005 *vol.* %. The different ranges of BNNTs' mass fractions range from 0.005 *wt.* % to 0.02 *wt.* % with an increment of 0.005 *wt.* % were used in this study. Besides, different nanoparticle diameters ranging from 5nm, 100 nm, 200 nm, and 300 nm against pure water as presented in Table 1. While simulating those variables, some parameters must keep constant such as the volume fraction of 0.35 *vol.* %, mass fraction of nanotube 0.001 *wt.*% and 5 nm of nanotube diameter. These fixed parameters were used based on a previous reference study using the same nanotube and surfactant type (Shamsuddin et al., 2021). The range of volume fraction, mass fraction and the size of the nanotube selected was based on a previous study on using Boron nitrate nanotube with surfactant for thermal conductivity effect *(Gómez-Villarejo, Aguilar, Hamze, Estellé, & Navas, 2019)*. Therefore, the present result can relate to and compare the previous finding on the same variable range on thermal and hydraulic performance.

Table 1. Nanofluid variable

| Fluid	Definition of variable
Nanofluid with surfactant	Varying surfactant volume fraction: 0.005 *vol.* % to 0.035 *vol.* %, (increment 0.005 *vol.* %)
	Fix parameter: 0.001 *wt.* % of nanotubes in the base fluid and 5 nm of nanotube diameter

Nanofluid with nanotubes mass fraction	Varying nanotube mass fraction: 0.005 *wt.* % to 0.02 *wt.* % (Increment 0.005 *wt.* %) Fix parameter: 0.35 *vol.* % of surfactant in the base fluid and 5 nm of nanotube diameter
Nanofluid with nanotube size	Varying nanotube diameter: 5 nm, 100 nm, 200 nm, and 300 nm Fix parameter: 0.35 *vol.* % of surfactant in the base fluid and 5 nm of nanotube diameter

2.2   Computational domain

Since the model employed numerical analysis, this analysis began with the creation of 3D geometry. The geometry was created using computer-aided design to represent the numerical computational domain. The dimension of channels is 10 mm x 10 mm x 0.213 mm (length, *L* x width, *W* x substrate, *t*) as demonstrated in Figure 1 and the dimension presented in Table 2. The material assigned to this channel was silicon rubber, as proposed by previous literature (Tuckerman & Pease, 1981). This analysis only considered a single symmetrical channel, as proposed by Husain and Kim (2008). This simplified model was used because it has a symmetrical effect on the opposite side of the domain. Therefore, the model can reduce the computational load and the time for numerical simulation to compute. Upon successfully obtaining optimum mesh size or suitable representative cell length, CFD analysis proceed with α and β so that this analysis can be made comparable with previous study.
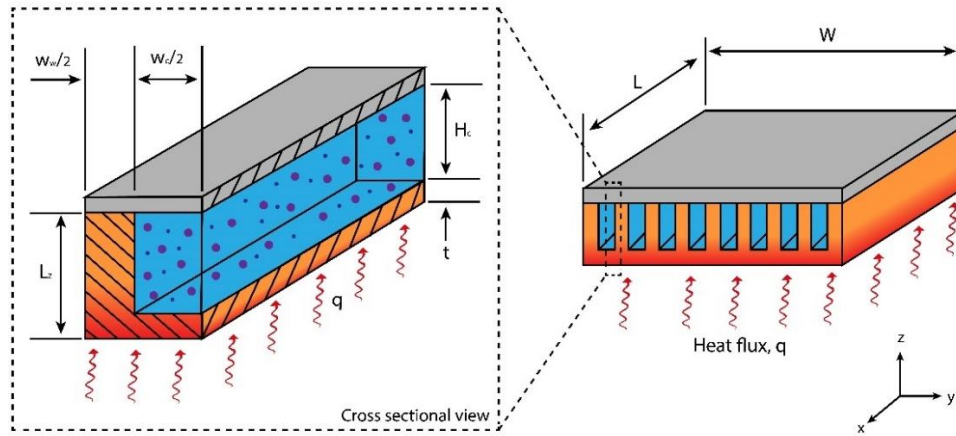
Figure 1. Simplified microchannel heat sink model

Table 2. Design variable and constrain.

Design variables	Value
Channel aspect ratio, α	5.218
Wall width ratio, β	1.0
Heat sink width, W (cm)	1.0
Heat sink length, L (cm)	1.0
Substrate thickness, t (mm)	0.0213
Channel height, H_c (mm)	0.032

2.3   Thermophysical properties of the nanofluid

In this study, few assumptions have been made about the fluid property acting as a single-phase and homogeneous flow between the base fluid and nanoparticle to reduce computational load. Therefore, the nanofluid's properties depend on the base fluid's temperature, as shown below (Alfaryjat, Mohammed, Adam, Stanciu, & Dobrovicescu, 2018; Ghasemi & Aminossadati, 2010).

9

$$\rho_{bf} = \frac{\begin{matrix} 999.84 + 18.225\,(T+273.15) - 7.92\ x\ 10^{-3}\ (T+273.15)^2 - \\ 5.545\ x\ 10^{-5}\ (T+273.15)^3 + 1.498\ x\ 10^{-7}(T+273.15)^4 \\ -3.933\ x\ 10^{-10}(T+273.15)^5 \end{matrix}}{1 + 1.816\ x\ 10^{-2}(T+273.15)} \tag{1}$$

$$\mu_{bf} = 2.414\ x\ 10^{-5}\ x\ 10^{\frac{247.8}{T-140}} \tag{2}$$

$$Cp_{bf} = 8958.9 - 40.535T + 0.11243T^2 - 1.014\ x\ 10^{-4}T^3 \tag{3}$$

$$k_{bf} = -0.58166 + 6.3556\ x\ 10^{-3}T - 7.964\ x\ 10^{-6}T^2 \tag{4}$$

In the present study, Boron nitride nanotube (BNNT) was used as a nanoparticle because its good thermal conductivity and properties are comparable to Carbon nanotube (CNT). Therefore, the thermophysical properties of the nanofluid depend on the nanotube volume fraction, $\emptyset$. The properties can be obtained using the equation below (Alfaryjat et al., 2018).

$$\rho_{nf} = (1 - \emptyset) \cdot \rho_{bf} + \emptyset \rho_{np} \tag{5}$$

$$\rho_{nf} Cp_{nf} = (1 - \emptyset) \cdot \rho_{bf}\, Cp_{bf} + \emptyset \rho_{np} Cp_{np} \tag{6}$$

The thermal conductivity can be calculated using empirical correlation of Brownian motion as given below.

$$k_{eff} = k_{static} + k_{Brownian} \tag{7}$$

The static thermal conductivity is given by

$$k_{static} = k_{bf} \left[\frac{k_{np} + 2k_{bf} - 2(k_{bf} - k_{np})\emptyset}{k_{np} + 2k_{bf} + (k_{bf} - k_{np})\emptyset} \right] \tag{8}$$

The Brownian thermal conductivity is given as

$$k_{Brownian} = 5\ X\ 10^4 \beta \cdot \emptyset \cdot \rho_{bf} \cdot Cp_{bf} \sqrt{\frac{\sigma_B \cdot T}{\rho_{np}.d_{np}}} \cdot f(T, \emptyset) \tag{9}$$

$$f(T, \emptyset) = \left(2.8217\ x\ 10^{-2} \cdot \emptyset + 3.917\ x\ 10^{-3} \left(\frac{T}{T_o} \right) + \right.$$

$$\left. (-3.0699\ x\ 10^{-2} \cdot \emptyset - 3.91123\ x\ 10^{-3}) \right. \tag{10}$$

The Boltzmann constant is represented by σ_B and β is the fraction of fluid volume fraction with moving nanoparticles.

$$\mu_{eff} = \mu_{static} + \mu_{brownian} \tag{11}$$

$$\mu_{static} = \frac{\mu_{bf}}{(1-\emptyset)^{2.5}} \tag{12}$$

$$\mu_{Brownian} = 5 \times 10^4 \beta \cdot \emptyset \cdot \rho_{bf} \cdot \sqrt{\frac{\sigma_B \cdot T}{\rho_{np} \cdot d_{np}}} \cdot f(T, \emptyset) \tag{13}$$

In which, d_{np} is represented by the nanotube diameter in the nanofluids. The thermophysical properties of the base fluid and nanoparticles were conducted at a reference temperature of 30°C.

Table 3. Thermophysical properties of working fluid (Gómez-Villarejo et al., 2019)

Thermophysical properties	Water	BNNTs	Triton X-100
Density (kg/m³)	998.2	1396.6	1070
Dynamic viscosity μ (Pa.s)	0.001	1.72×10^5	0.027
Thermal conductivity k (W/m.K)	0.60	46	0.252
Specific heat Cp (J/kg.K)	4182	1225	2415

2.4 Governing Equation

This numerical CFD simulation involved fluid flow and heat transfer processes under a steady state. The incompressible flow was modelled using the steady-state assumption. Governing equations were required for the numerical domain: Mass, momentum, and energy conservation (Taylor, 2011) for heat transmission through convection in the microchannel. The equation may be expressed as a tensor, as seen below.

Conservation of Mass:

$$\frac{\partial \rho_f}{\partial t} + \frac{\partial \rho_f u_i}{\partial x_i} = 0 \qquad (14)$$

Conservation of Momentum:

$$\rho_f \frac{\partial u_i}{\partial t} + \rho_f \frac{\partial u_i}{\partial x_j} = -\frac{\partial p}{\partial x_i} + \rho_f g_i + \frac{\partial}{\partial x_j}\left(\mu_f \frac{\partial u_i}{\partial x_j}\right) + \frac{\partial}{\partial x_j}\left(\mu_f \frac{\partial u_j}{\partial x_i}\right) - \frac{2}{3}\frac{\partial}{\partial x_j}\left(\mu_f \frac{\partial u_k}{\partial x_k}\right) = 0 \qquad (15)$$

Conservation of Energy:

$$\rho_f \frac{\partial h}{\partial t} + \rho_f u_j \frac{\partial h}{\partial x_i} = \frac{\partial p}{\partial t} + u_i \frac{\partial p}{\partial x_i} + \frac{\partial}{\partial x_i}\left(k_f \frac{\partial T_f}{\partial x_i}\right) + \tau_{ij} \frac{\partial u_i}{\partial x_j} \quad \text{(Fluid domain)} \qquad (16)$$

$$\frac{\partial}{\partial x_i}\left(k_s \frac{\partial T_s}{\partial x_i}\right) = 0 \quad \text{(Substrate conduction)} \qquad (17)$$

The mathematical formulation requires solving boundary conditions repeatedly in each cell centroid, as presented in Table 4. A homogeneous heat flux (q), 790 W/cm^2, was assigned at the bottom wall of the heat sink. This heat flux was assumed to be homogenous as the surface area contact between the heat source and the nanofluid consist of the substrate and t distance between them. This substrate would distribute heat evenly before reaching the nanofluid. Besides, the inlet temperature was varied from 10 ℃ to 70 ℃ to investigate the effect of different temperature ranges. In addition, the mass and volume fraction range began from 0.005 wt % to 0.02 wt % and 0.05 vol% to 0.35 vol % experimental validation on the thermal property. Most outside walls were believed to be completely insulated from the computational domain. The x and z coordinates of the heat sink planes are subjected to symmetrical boundary requirements. The fluid flow rate and the temperature entering the microchannel are 4.7 cm^3/s and 30°C, respectively.

In contrast, the channel outlet has a constant static pressure barrier condition. Temperature and heat flow continuity are the conjugate boundary conditions connecting the fluid and wall energy equations. Equations (14) - (17) were numerically solved ==using a finite volume CFD solver with the aid of Ansys Fluent.== The simulation was completed when the residual values for all the governing equations used achieved minimum criteria, below 1 x 10^{-6} with constant error.

Table 4. Setup of CFD boundary condition

Boundary condition	Value
Analysis type	Steady-state (Hong, Cheng, Ge, & Joo, 2007)
Type of flow	Laminar (Hong et al., 2007)
Number of cycles	400
Ambient & Inflow temperature	30 ℃ (Halelfadl et al., 2014)
Inlet flux	4.7 cm^3/s (Halelfadl et al., 2014)
Outlet flux	0 Pa
Heat flux	790 W/cm^2 (Tuckerman & Pease, 1981)
Pressure correction type	SIMPLE method (Hong et al., 2007)

2.5 *Data acquisition*

In this section, the geometrical ratio was represented by the channel aspect ratio, α and wall width ratio, β was fixed throughout this study. The thermal and hydraulic performance and standard dimensionless parameters of the microchannel heat sink (MCHS) were defined below. The geometrical ratio (Shamsuddin et al., 2021) begins with α as seen below.

$$\alpha = \frac{H_c}{W_c} \tag{18}$$

The channel aspect ratio, α is defined as the ratio of channel height to channel width.

$$\beta = \frac{W_w}{W_c} \tag{19}$$

The wall width ratio β is represented by the ratio of wall width to channel width. Besides of geometrical ratio, the calculation of thermal resistance (Leng, Wang, Wang, & Yan, 2015) can be seen below.

$$R_{th} = \frac{\Delta T_{max}}{q A_s} \tag{20}$$

whereas A_s is the heat flux substratum area, and ΔT_{max} is the maximum heat sink temperature rise defined as,

$$\Delta T_{max} = T_{s,o} - T_{f,i} \tag{21}$$

The pumping power required to move the fluid flow throughout the microchannel cavity is given below (Shen et al., 2017).

$$\bar{P} = n \cdot u_{avg} \cdot A_c \cdot \Delta p \tag{22}$$

The pressure drop, Δp, and the average flow velocity, u_{avg} are used to calculate the Reynold number, Re, as below.

$$Re = \frac{\rho u_{avg} D_h}{\mu} \tag{23}$$

The Reynold number represents the ratio of inertial force to viscous force. ρ is density, μ is the absolute viscosity, and D_h is the hydraulic diameter given as below.

$$D_h = \frac{2 H_c W_c}{H_c + W_c} \tag{24}$$

The Nusselt number (Nu) represents the ratio of thermal convection to the thermal conductivity of the nanofluid, as represented below

$$Nu = \frac{h D_h}{k} \tag{25}$$

Where h is convection heat transfer and k is conduction heat transfer.

2.6   Boundary conditions

2.6.1   Inlet boundary condition of a microchannel

Assumption of laminar flow was used throughout the study since the Reynold number was below 700. Therefore, the inlet velocity is defined as below.

$$V_{inlet} = \frac{\dot{m}}{\rho A_s} \tag{26}$$

The cross-sectional area represented by A_s and the mass flow rate of the fluid is represented with $\dot{m}$.

2.6.2   Outlet boundary condition

Static pressure is assigned outlet section of the microchannel heat sink. The static pressure is assumed to be atmospheric pressure.

2.6.3   Wall boundary condition

No-slip condition for fluid flow was applied to inside - channel wall of the microchannel heat sink. In addition, an adiabatic condition was assigned at the top section of the microchannel to ensure the direct effect of heat losses from convective heat transfer of fluid flow.

2.7   Mesh sensitivity test

This study employed the finite volume method to solve the solution iteratively. The accuracy of the solution relies on the size of the mesh. The smallest mesh provided the highest accuracy. However, the situation may increase the computational load and make it time-

consuming. Therefore, the selection of optimum mesh size balances solution accuracy and low computational load. In addition, mesh refinement between solid and fluid layers needs to be defined to capture viscous sublayer flow region with *y+* less than 5 (Singh, Rudman, & Blackburn, 2017). Therefore, the model utilized a growth rate of 1.2, and the first mesh thickness near the wall was 0.005 mm. After the first layer thickness was established, a mesh sensitivity test was conducted to provide the highest mesh accuracy (Mat, Asmuin, Basir, Abbas, et al., 2021; Mat et al., 2020; Mat, Asmuin, Basir, Safaei, et al., 2021). In this test, ten different meshes were generated. That generated mesh was identified as representative cell length. The representative cell length is the ratio of mesh size over characteristic length. The characteristic length for the case of a microchannel is 1 cm. Three mesh were chosen from those generated meshes as coarse, medium, and fine mesh that begins with the first trial. The process was repeated a few times until the value of extrapolated error was below 5%. The extrapolated error is the relative difference between an extrapolated solution and a numerical solution. The extrapolated value was calculated using the Richardson Extrapolation method (Roache & Knupp, 1993). Based on the generated result, as shown in Figure 2, the selected optimum representative cell length that gives acceptable numerical accuracy is 1.2×10^{-5}. This length was used for the data validation study in the next section.
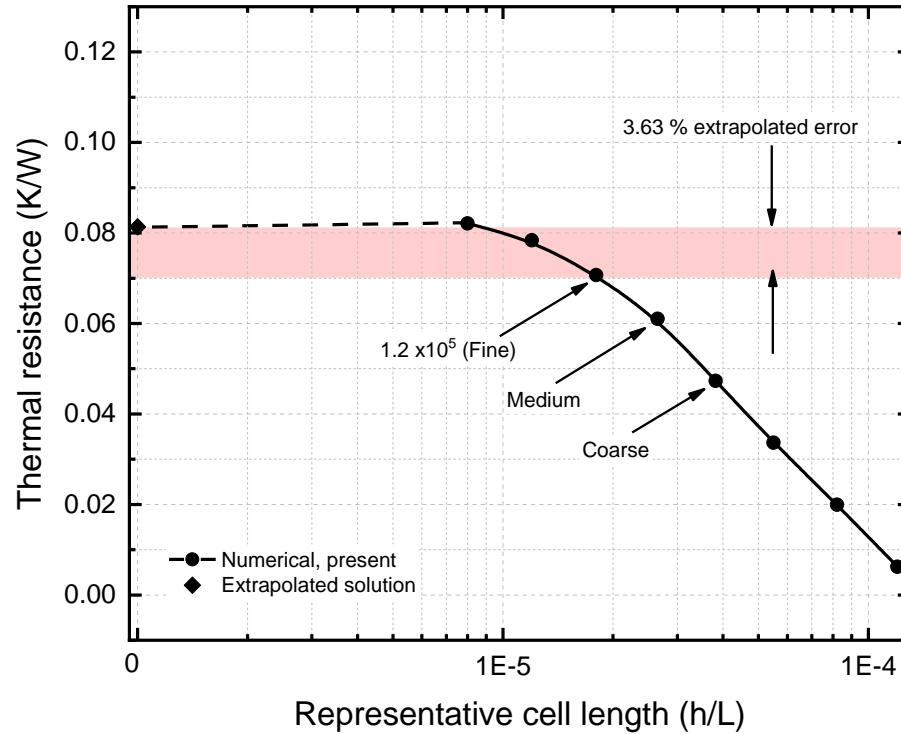
Figure 2. Mesh sensitivity test

2.8   *Validation study*

<mark>The working fluid used in this study was water base to validate the computational domain of the microchannel geometry. The range of Reynold numbers from the lowest to the highest (200 – 800) to justify the behaviour in a computational domain.</mark> The numerical simulation measured thermal resistance, as shown in Figure 3 and pressure drop, as presented in Figure 4, over different Reynold numbers (*Re*). Based on Figure 3, the relative error increases with an increase of *Re*. The reason was probably due to viscous-sub layer approximation error as the value depends on flow velocity. From the graph, the maximum relative error is around 5% at Re of 700. Besides comparing the heat transfer coefficient, the numerical validation was conducted on the second parameter, pressure drop, as shown in Figure 4. Based on the graph, the relative errors increase with *Re* increases, and the numerical simulation value over-predicted the

17

experimental result (Lee & Mudawar, 2007). Based on the graph, the maximum relative error is approximately 4% at Re of 800. Therefore, based on the data validation study, the numerical computation solution was promised for this study.
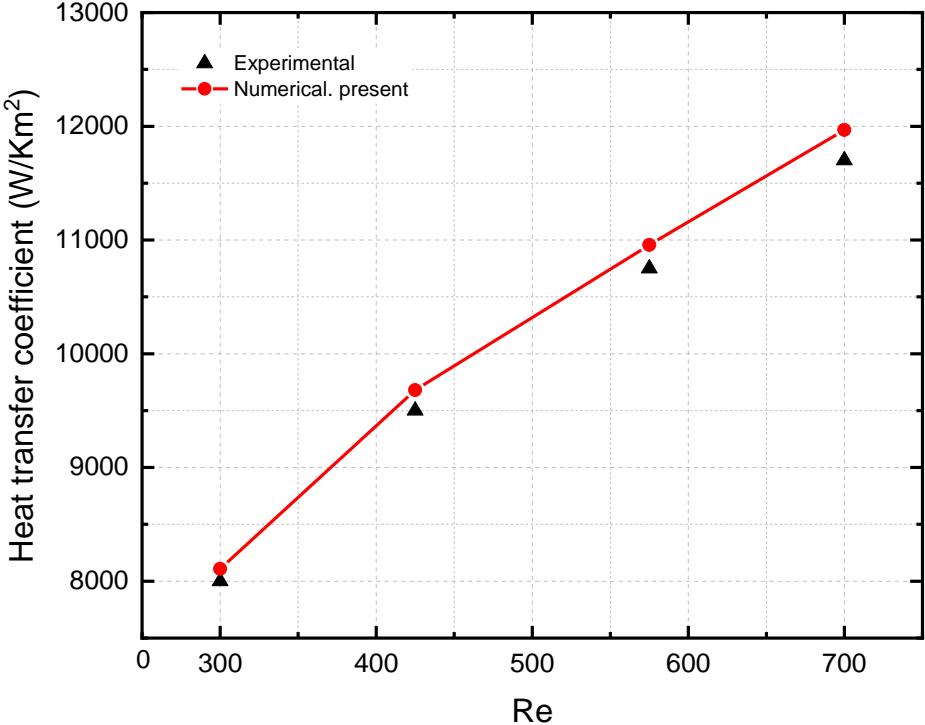
Figure 3. Validation of heat transfer coefficient
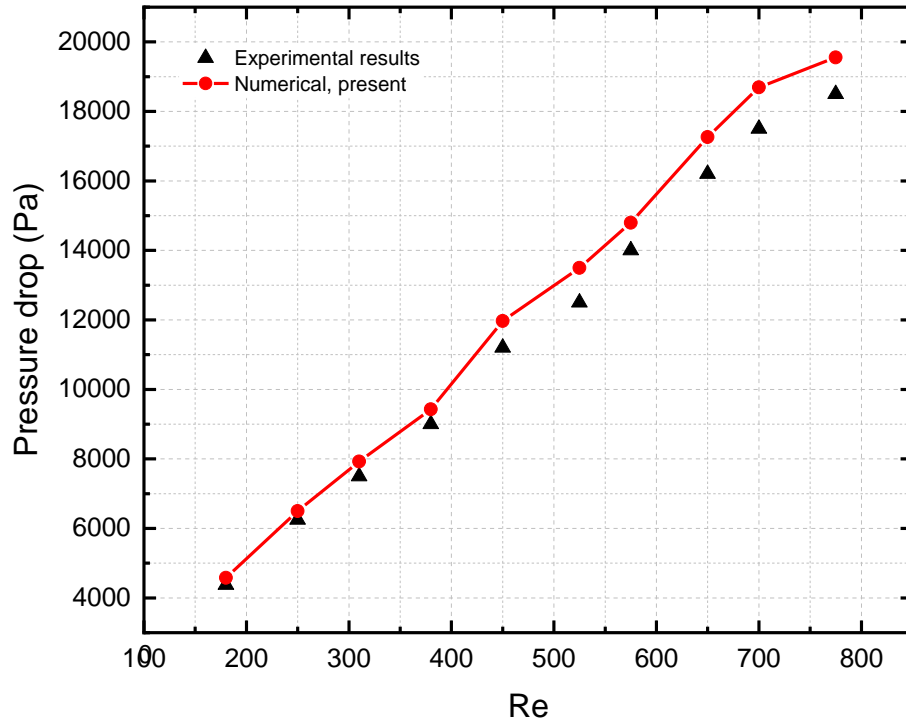
**Figure 4.** Validation on pressure drop

3.0   Result and discussion

With numerical accuracy confirmed, thermal and hydraulic performance effects were investigated on different surfactant volume fractions, nanoparticle mass fractions and nanotube diameter against pure water. In particular, those performances were analyzed on a specific range of *Re* and temperature 300 – 700 and 10 ℃ – 70 ℃, respectively. These ranges were chosen for comparison purposes with the previous literature review. This section introduces the flow pattern to add a better understanding of the flow interaction and interpretation.

3.1   *Flow pattern*

The inlet velocity inside the microchannel heat sink (MCHS) increases with the increment of volume fraction, as presented in Figure 5. The reason is that adding more volume fractions will increase the fluid viscosity, directly related to Eq. 23. As a result, fluid moves with lower velocity. Lower velocity may cause a long entrance as the fluid takes time to develop. The development flow can be seen in figure 6. In the figure, velocity streamline start to develop after the fully develop flow as shown in the inlet section. Pure water alone has the largest entrance length, reflecting the delay in flow development. The delay in flow development affects the time for heat absorption by convective heat transfer. In addition, the velocity streamlines embedded in the same velocity contour plot show that the wall's velocity streamlines are closed to each other for all ranges of volume fractions. Figure 7 presents the temperature distribution inside the microchannel heat sink. Flow development plays a crucial role in the effective heat enhancement process. At the flow entrance, fluid begins to absorb the heat as compared to pure water alone. Due to this, adding nanoparticles and stabilizing them with surfactant help distribute the heat evenly from the entrance to the outlet section. Apart from that, pressure distribution along the channel can be seen in Figure 8. As expected, the lowest pressure can be seen at the channel's entrance for the pure water, while the base fluid with surfactant and nanotubes contributed to the largest pressure drop in the channel. This is because the viscosity of pure water is lesser than that of nanofluid. Thus, this influenced the pressure drop. Based on the result, further investigation was needed to analyze the effect of thermal and hydrodynamic performance for clear data interpretation.
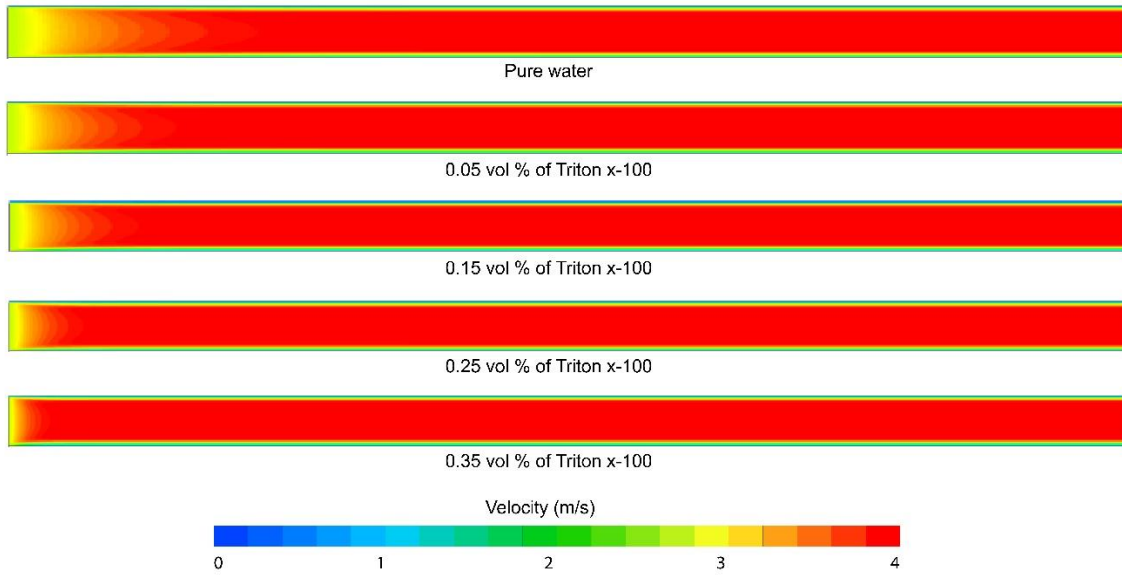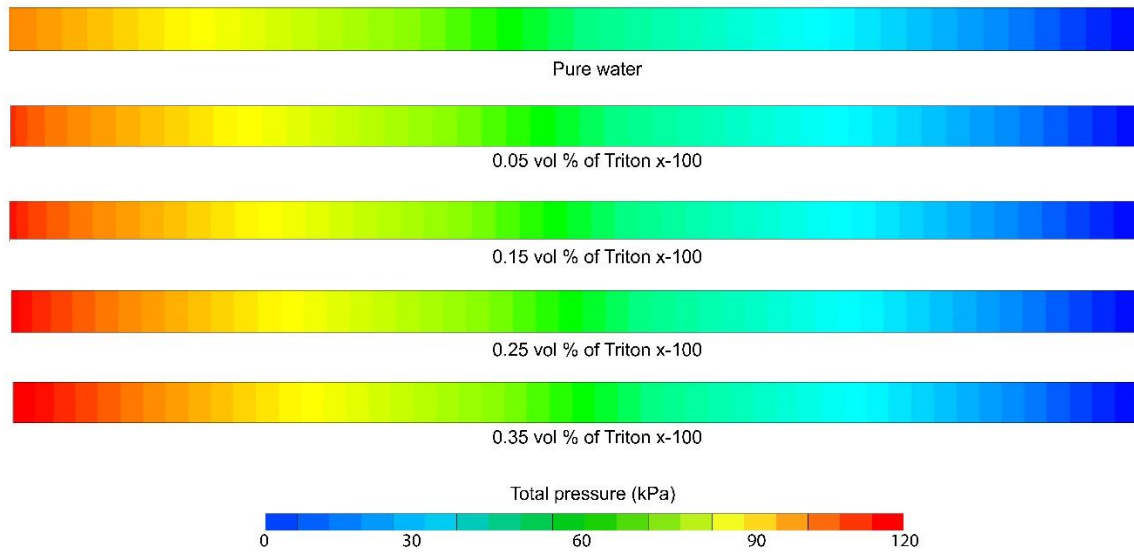
Figure 5. Velocity contour plot for different TX-100 volume fraction
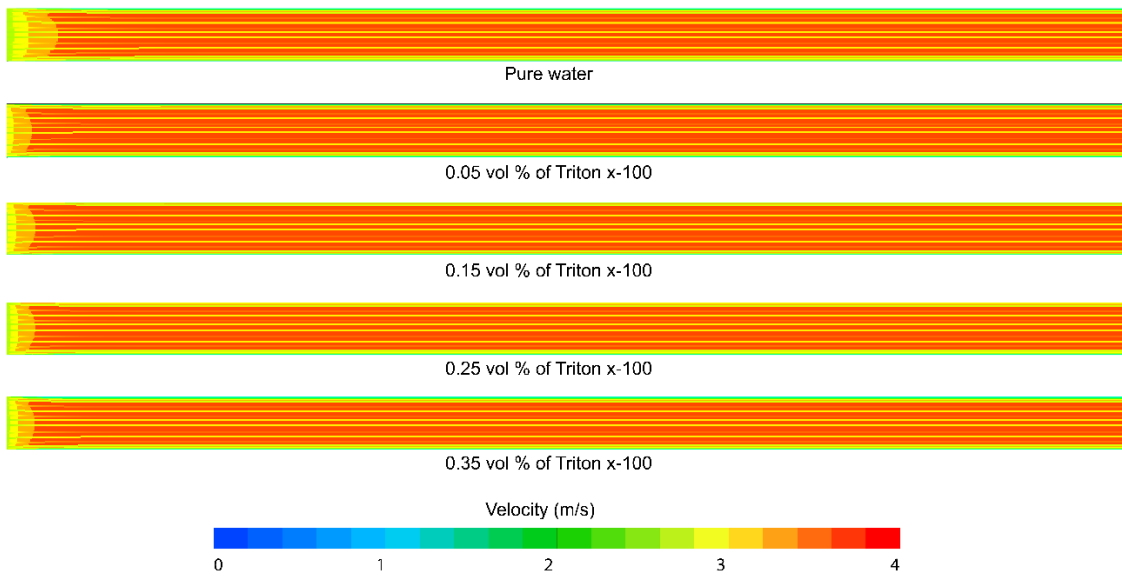
Figure 6. Velocity streamline for different TX-100 volume fraction
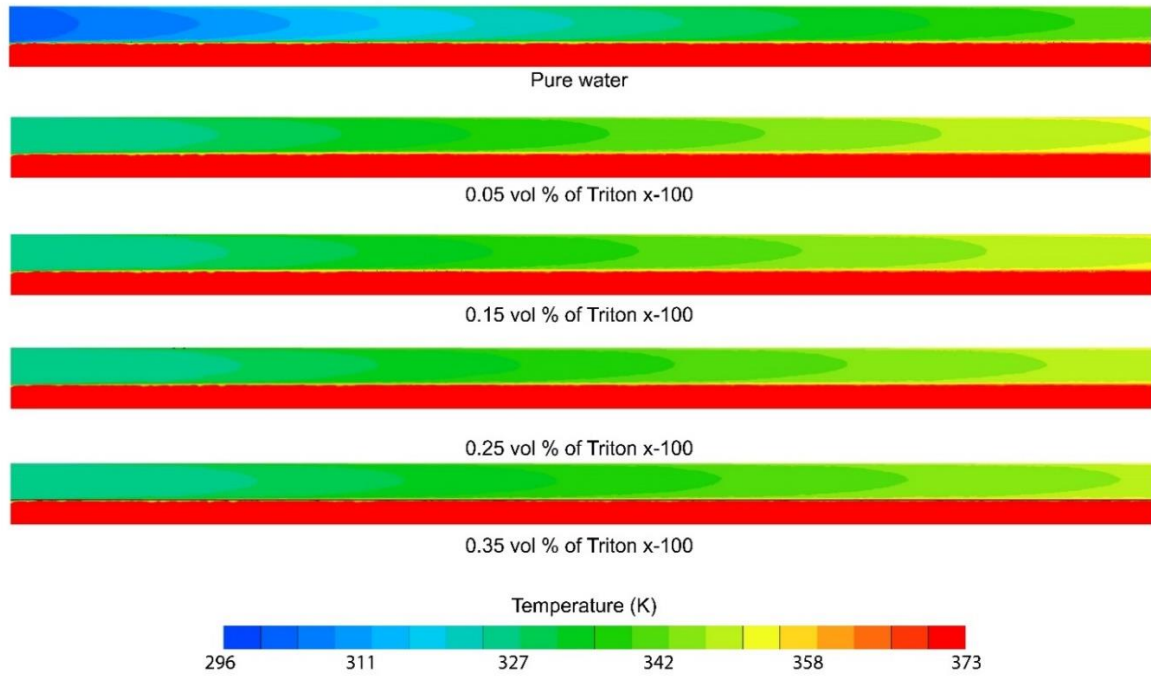
Figure 7. Temperature contour plot for different TX-100 volume fraction

Figure 8. Total pressure contour plot for different TX-100 volume fraction

3.2   Thermal performance

3.2.1   Thermal resistance

Thermal resistance inside the microchannel heat sink (MCHS) increases with the *Re* in all cases, as seen in Figure 9. Additional Triton TX-100 surfactant and Boron Nitride nanoparticle in nanofluid leads to better heat transfer enhancement. The reason is probably due to the additional substances that act as heat carriers to disperse heat evenly inside MCHS's cavity. Due to the dispersion functionality of these substances, this causes the nanofluid provides better heat transfer performance. Hence, the usage of nanofluid and surfactant in a base fluid is increasing for better heat thermal management. It is also expected that the demand for these substances continues to grow along with complex advancements in the heat transfer process and higher heat flux capacity, which water alone is unable to sustain. Because of the superiority of this substance, further investigation was carried out to reveal further the impact of different concentrations of these substances: nanofluid, surfactant and the size of nanotube diameter. Increasing surfactant concentration in the nanofluid reduced the thermal resistance in the microchannel heat sink. The maximum drop in the thermal resistance with the other surfactant concentration was reported at approximately 90 % as a reference of the pure water for 0.35 *vol* % surfactant across all the *Re,* as seen in Figure 9a. In contrast, the lowest surfactant concentration contributes less thermal resistance to the microchannel. The reason is that the nanofluid obtains stability because surfactant effect (Khairul, Shah, Doroodchi, Azizian, & Moghtaderi, 2016). This additional surfactant prevents the nanoparticle from particle agglomeration as it acts as anti-surface tension between particle to particle. Figure 8b presents the effect of nanoparticle concentration ranging between 0.005 *wt*.% to 0.02 *wt*.% with an increment of 0.005 wt.%. The thermal resistance was reduced with a further increase in nanoparticle mass fraction. The

maximum drop for thermal resistance was twice as compared with the pure water for 0.02 *wt*.%

for all ranges of the *Re,* as demonstrated in Figure 9b. Despite this, the smallest nanoparticle

concentration gives the lowest drop in the thermal resistance, around 50% for 0.005 *wt*.%. This

additional nanoparticle concentration enhances the heat transfer process due to the additional

conductivity effect of the solid nanoparticles. These nanoparticles absorb heat and disperse it in

the fluid evenly (Jebasingh & Arasu, 2020). Figure 9c presents the effects of thermal resistance

on different sizes of nanoparticle diameter ranging from 5nm to 300 nm. A significant effect of

introducing different sizes of nanoparticles was reported on improving the heat transfer process

in the microchannel. The small size of the nanoparticle reduces the thermal resistance by as

much as twice as compared to pure water alone. This is due to increased surface area contact

between particles for better heat conductivity (Ealia & Saravanakumar, 2017). Figure 10 presents

the effects of thermal resistance on temperature with various concentrations of nanotubes in the

base fluid. As expected, the thermal resistance rises with a further increase in inlet fluid

temperature for all the cases, as demonstrated in Figure 10a. The correlation also can be seen in

Eq. (20). The significant finding reveals that the maximum dropping in the thermal resistance

was around 75% for 0.35 *vol*. % surfactant concentration as a reference to pure water across all

ranges of temperature. This may be due to the specific heat capacity of the nanofluid. As

indicated in Eq. (20) following Eq. (21), these equations illustrate that the thermal resistance

increase with an increased temperature difference between the wall and fluid temperature. Figure

10b demonstrates the effect of thermal resistance on temperature with different mass fractions of

the nanoparticle. The critical finding reveals that the lowest temperature of nanofluid contributes

the lowest thermal resistance, approximately around 70 K/mW for 0.005 *wt* % at 10 ℃, as shown

in Figure 10b. At the same time, the lowest thermal resistance for different sizes of nanoparticles

was reported at around 80 K/mW for 0.005 *wt.* % at 10 ℃, as seen in Figure 10c. However, the effects of concentration for the surfactant and the nanofluid are quite complicated. Pure water seems to be more advantageous than adding those substances in minimizing thermal resistance for temperatures less than 303 K, as shown in Figure 10a and Figure 10b. Since the little effect of those concentrating substance on thermal performance, all concentration provides as high as 24% and 12% more thermal resistance than pure water alone at the temperature of 280 K and 290 K, respectively. In contrast, at a temperature of more than 303 K, different concentration of those substances greatly minimizes thermal resistance compared with pure water. Therefore, it can be summarized that altering the concentration of the surfactant, the nanofluid, and its diameter provides optimal thermal conditions for enhancing MCHS.
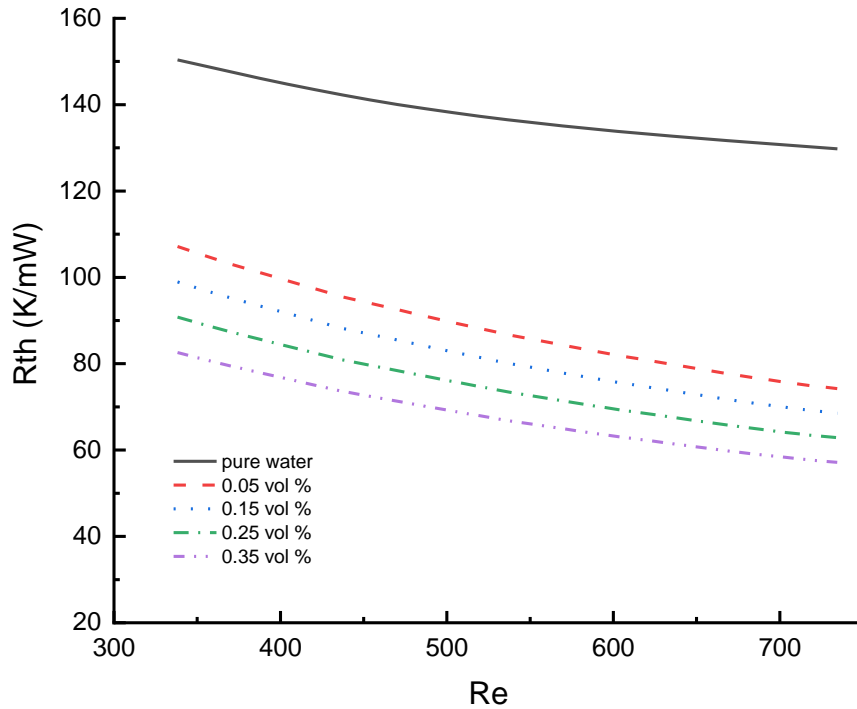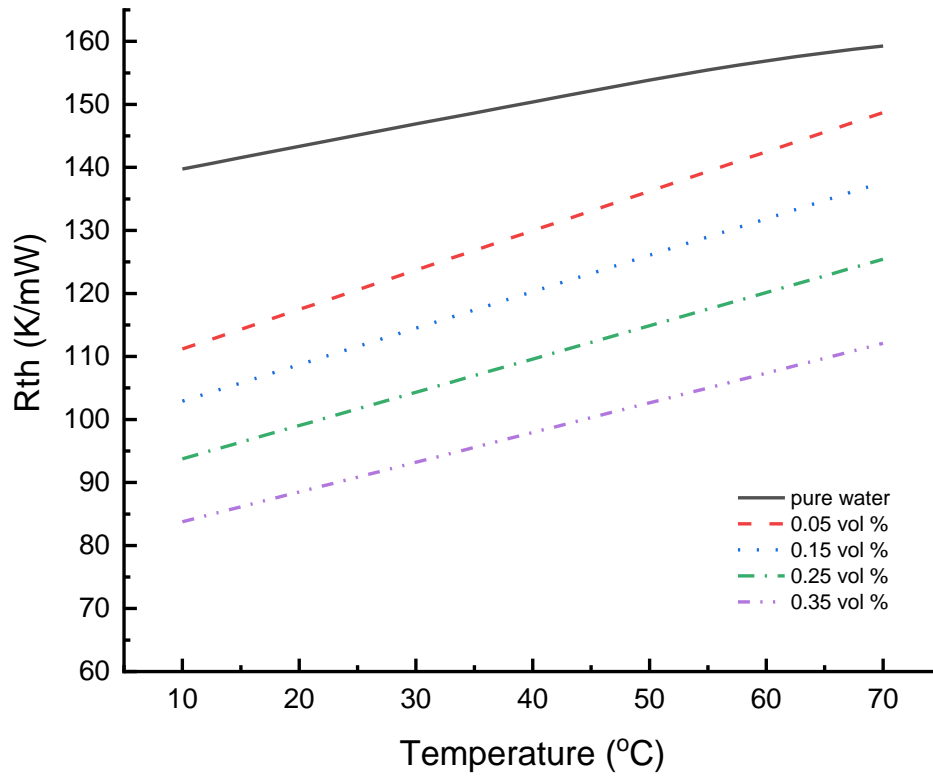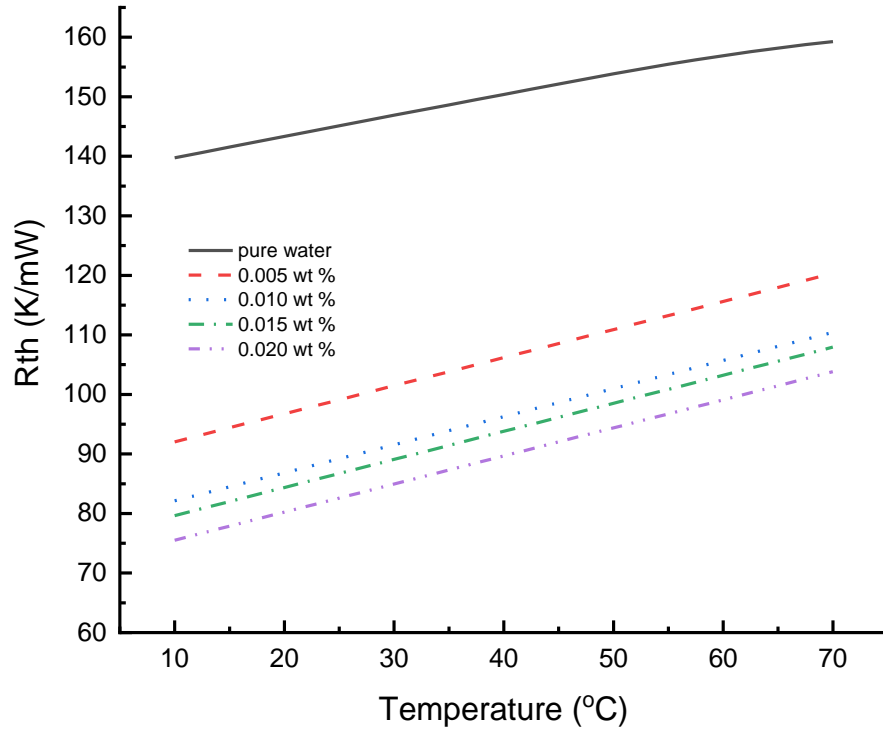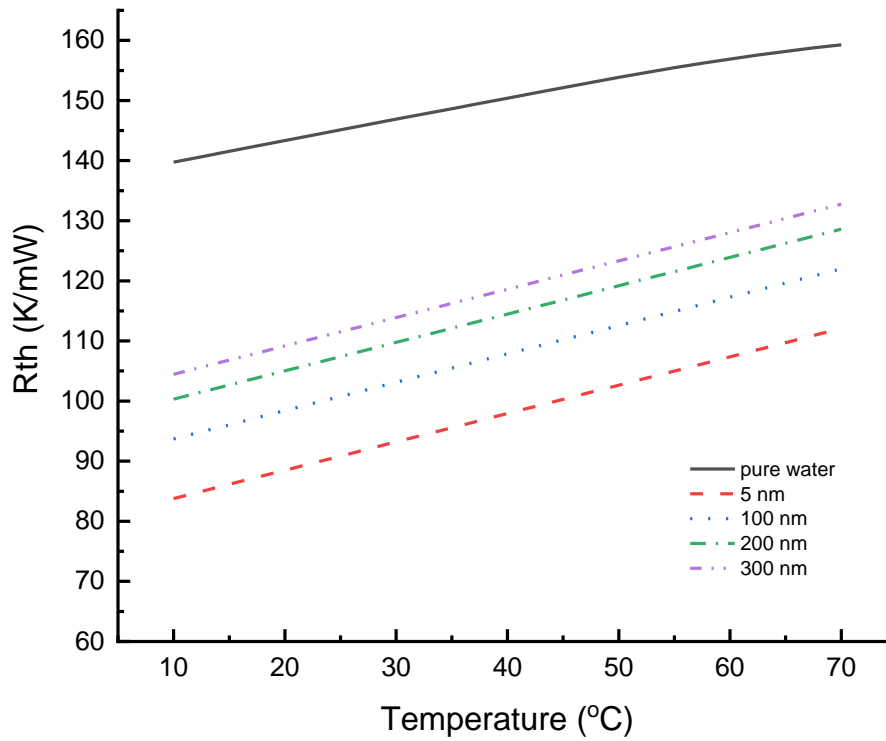

(a)
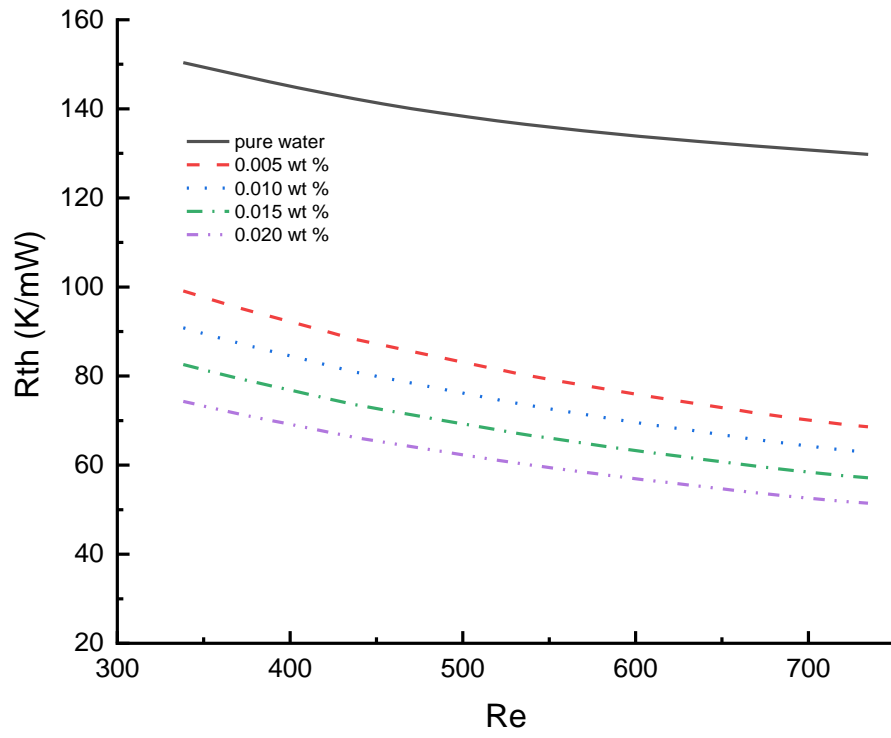
(b)
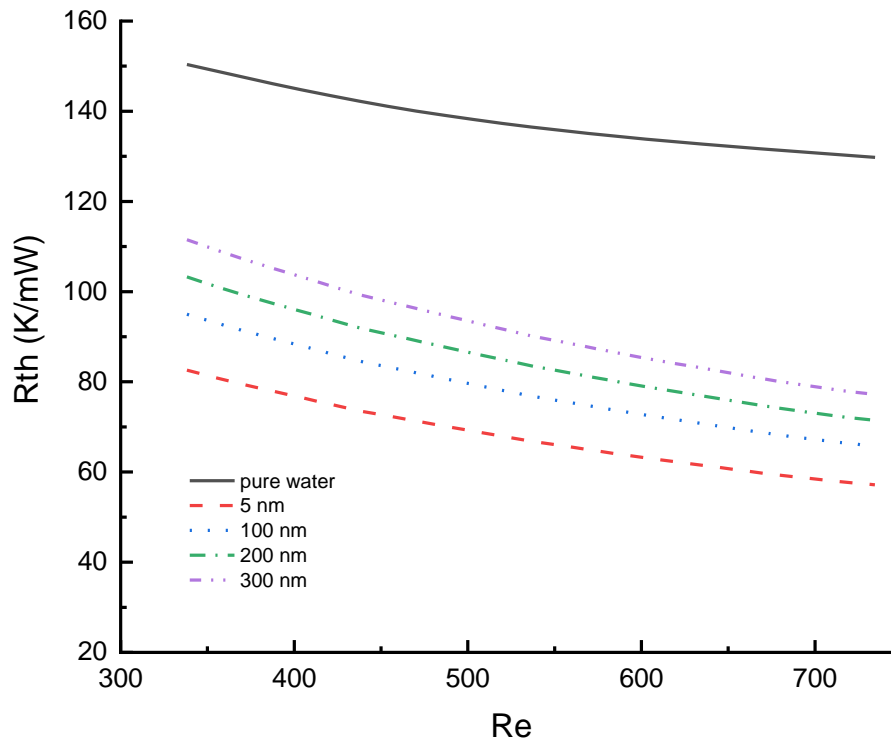
(c)

Figure 9. Effects of thermal resistance on *Re* with different of (a) TX-100 surfactant volume fraction, (b) BNNT nanoparticle mass fraction, and (c) size of nanoparticle diameter
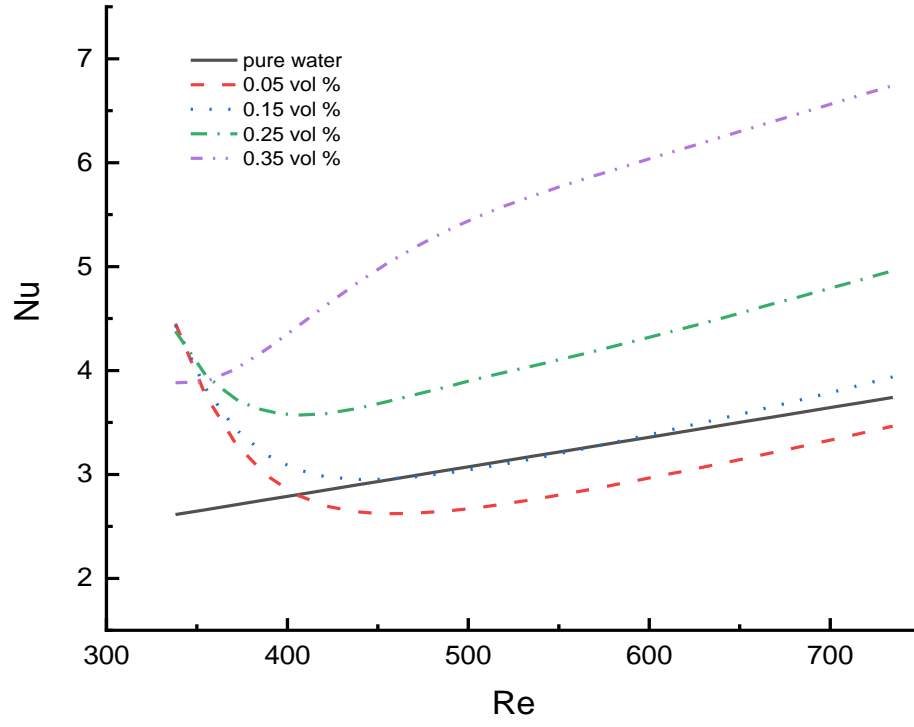

(a)

(b)

(c)

Figure 10. Effects of thermal resistance on temperature with different of (a) TX-100 surfactant volume fraction, (b) BNNT nanoparticle mass fraction, and (c) size of nanoparticle diameter
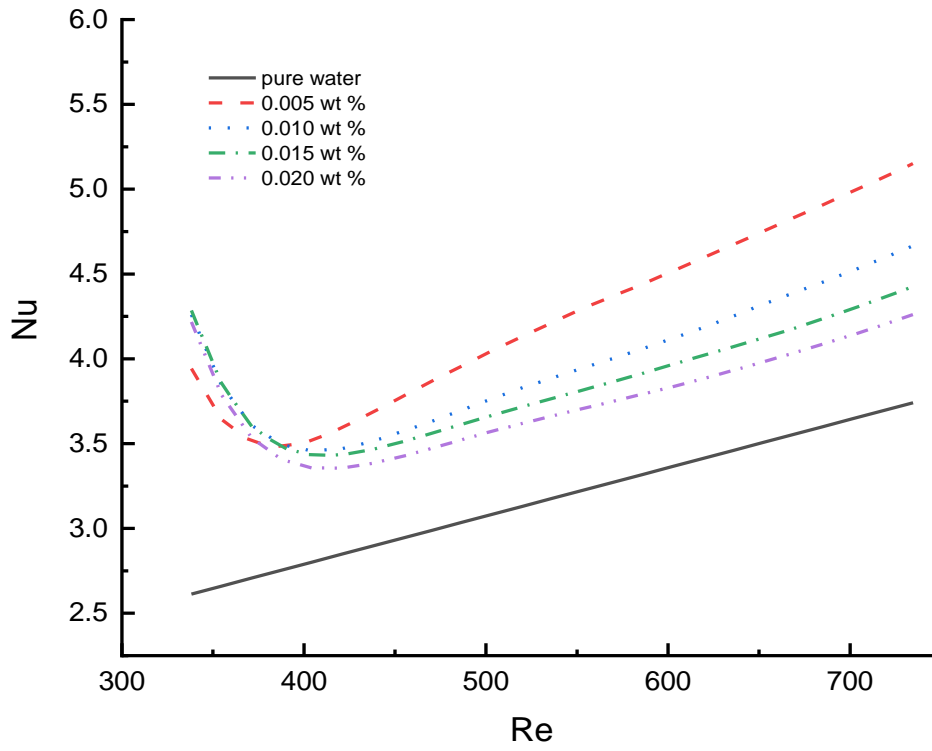
3.2.1   Nusselt number

An additional parameter for the thermal performance, Nusselt number (*Nu*), was introduced in this section. This *Nu* is a crucial parameter in investigating the ratio of convection heat transfer to conduction heat transfer for the nanofluid, as indicated in Eq. (25). Increasing the Reynold number (*Re*) increases the *Nu* for all the cases. This is due to most of the heat convection rather than the conductivity of heat transfer, as indicated in Eq. (25). Increasing flow velocity translates to frequency contact of fluid flow to the heat source. Thus, the heat transfer enhancement process (Esfe, Nadooshan, Arshi, & Alirezaie, 2018). Besides, the trend of different surfactant concentrations on *Nu,* as shown in Figure 10a, seems quite complicated. For instance, the surfactant volume fraction of 0.35 *vol.* % gave the lowest *Nu* as compared to other concentrations for the *Re* below 350. While after that point, the *Nu* for 0.35 *vol.* % increase more than other surfactant concentrations. However, significant finding reveals that 0.05 *vol.* % provides the lowest *Nu* as compared to others concentration and even lower than that the pure water. At the same time, the surfactant concentration that is comparable to pure water is 0.15 *vol.* % as the *Nu* characteristic is almost similar after the *Re* of 450. Figure 11b also seems to have a complex trend as the value of *Nu* contradicts before the *Re* of 400. The critical finding shows that a lower mass fraction of 0.005 *wt.*% provides a better heat transfer process than other mass fractions after the *Re* of 400. The lowest Nu was reported for the highest nanoparticle mass fraction of 0.02 *wt.* %. This finding is essential for evaluating the amount of nanoparticle concentration as this influences not only the *Nu* number but also thermal resistance performance.

Figure 11c demonstrates the effect of different sizes of nanoparticles in nanofluid on the *Nu*. The result shows an increasing size of nanoparticles will enhance the convection heat transfer process and the *Nu* as well. This is probably due to the smallest nanoparticles contributing to the largest quantity of nanoparticles that enhance the thermal conductivity of the fluid. Thus, Eq. (25) indicates that the thermal conductivity is inversely proportional to the *Nu*. The effect of *Nu* against inlet flow temperature is highly responsible at around 20 ℃, as shown in Figure 12. In addition, the effect of surfactant concentration in the nanofluid shows that increasing the surfactant concentration gives the highest *Nu* in the microchannel. Furthermore, adding a small amount of surfactant concentration still gives a better thermal performance as a reference to the pure water alone, as presented in Figure 12a. However, this is not the case for adding nanoparticle mass fraction into the nanofluid. The result shows that the least amount of nanoparticle mass, 0.005 *wt.* % contribute to the highest *Nu* and above the pure water. The rest of the mass fraction ranged from 0.01 to 0.02 *wt.* % gives the lowest *Nu* even less than the pure water, as shown in Figure 12b. The impact of nanoparticle size on the *Nu* against temperature can be seen in Figure 12c. Changing the particle size significantly influences the thermal performance in the microchannel. However, significant finding reveals that at the lowest temperature, the biggest nanoparticle has the largest nanoparticle size. It seems that the trend for the smallest particle size, 5 nm overperforms the *Nu* as compared to the rest of the nanoparticle size at 40 ℃.
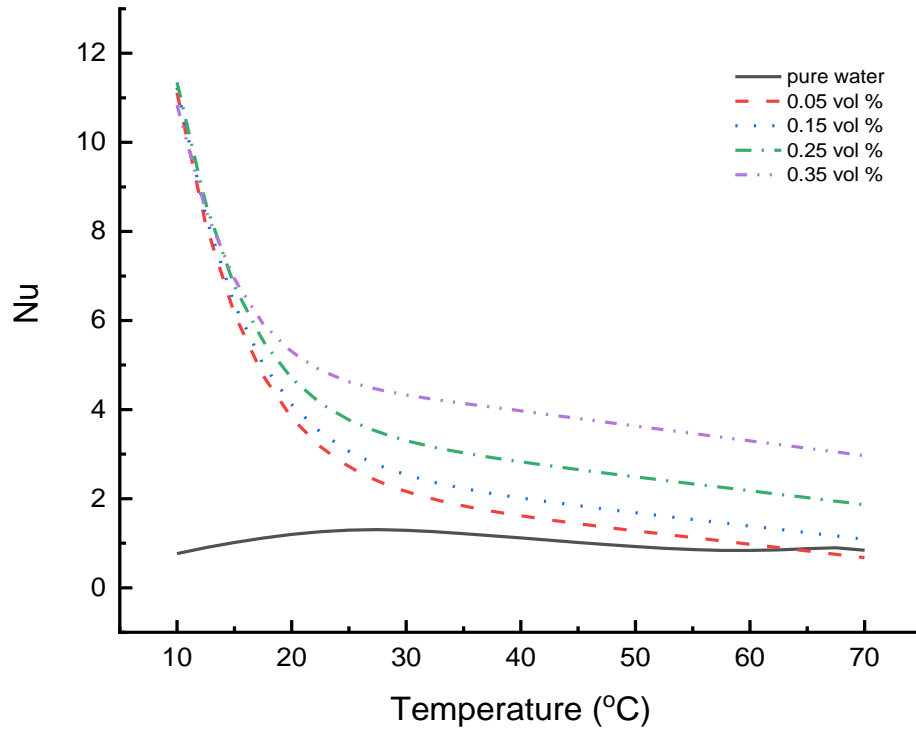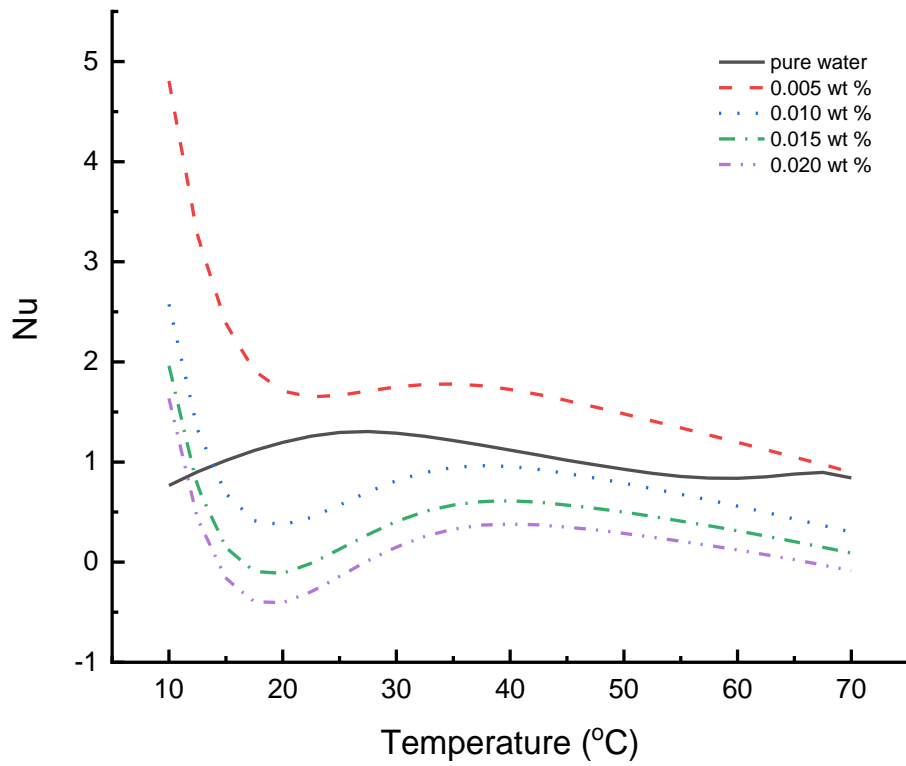
(a)

(b)

31
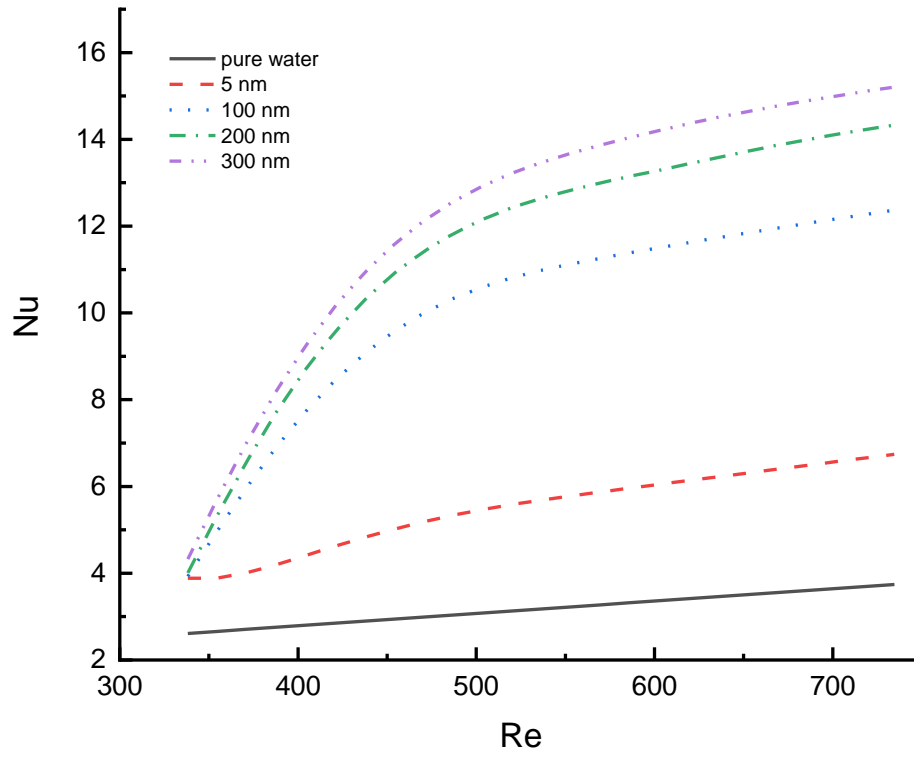
(c)

Figure 11. Effects of Nusselt number on Reynold number for different (a) TX-100 surfactant volume fraction, (b) BNNT nanoparticle mass fraction, and (c) size of nanoparticle diameter
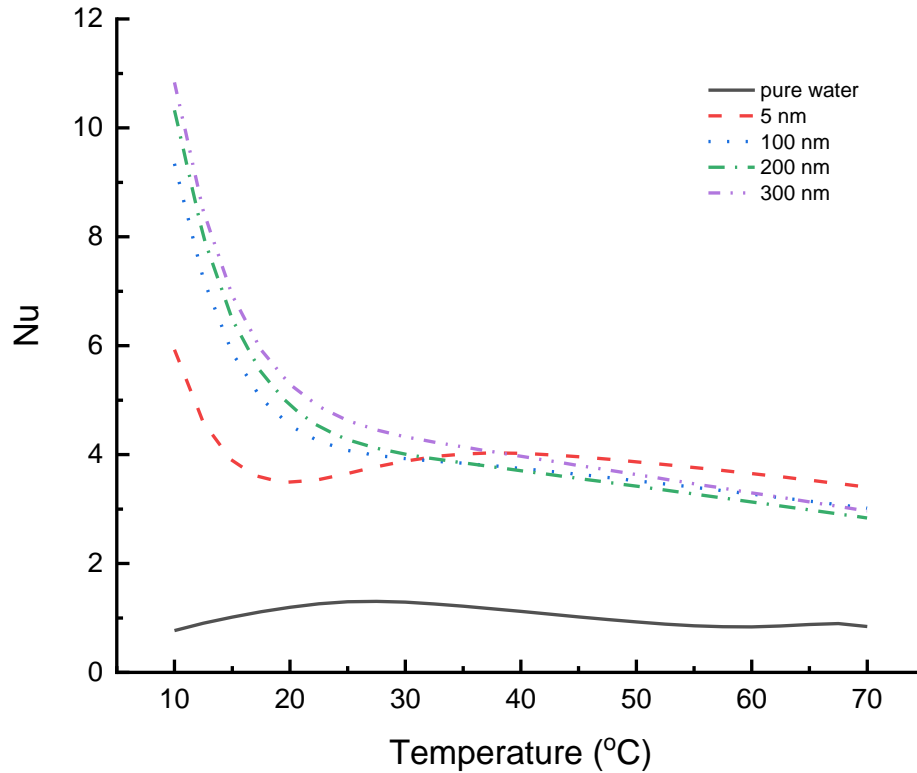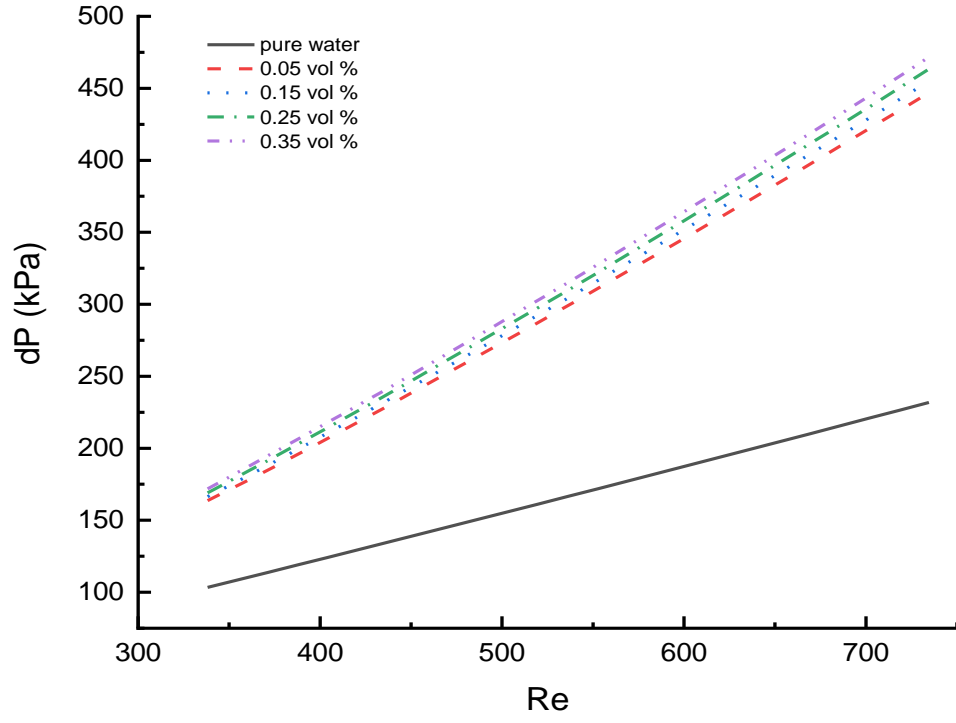
(a)

(b)

Figure 12. Effects of Nusselt number on temperature for different (a) TX-100 surfactant volume fraction, (b) BNNT nanoparticle mass fraction, and (c) size of nanoparticle diameter
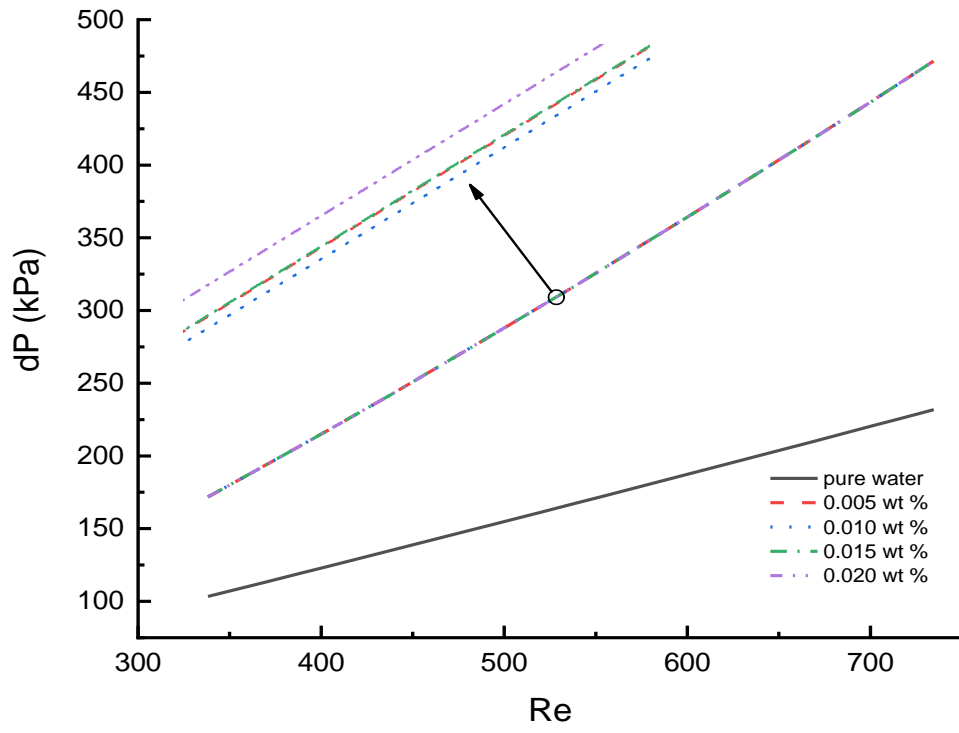
3.3   Pressure drop

The effects of pressure drop against Reynold number (*Re*) are presented in Figure 13. Increasing Re will almost linearly increase the pressure drop for all cases. This is because the *Re* is influenced by fluid flow velocity, as shown in Eq. (23). This velocity directly correlates with the pumping power and pressure drop, as indicated in Eq. (22). From this equation, increasing *Re* will increase the velocity leading to more pumping power requirement. More pumping power is required in this case because the fluid flow travels at high speed, leading to more friction across the MCHS channel. Since reducing pumping power is one of the keys to improving the MCHS,
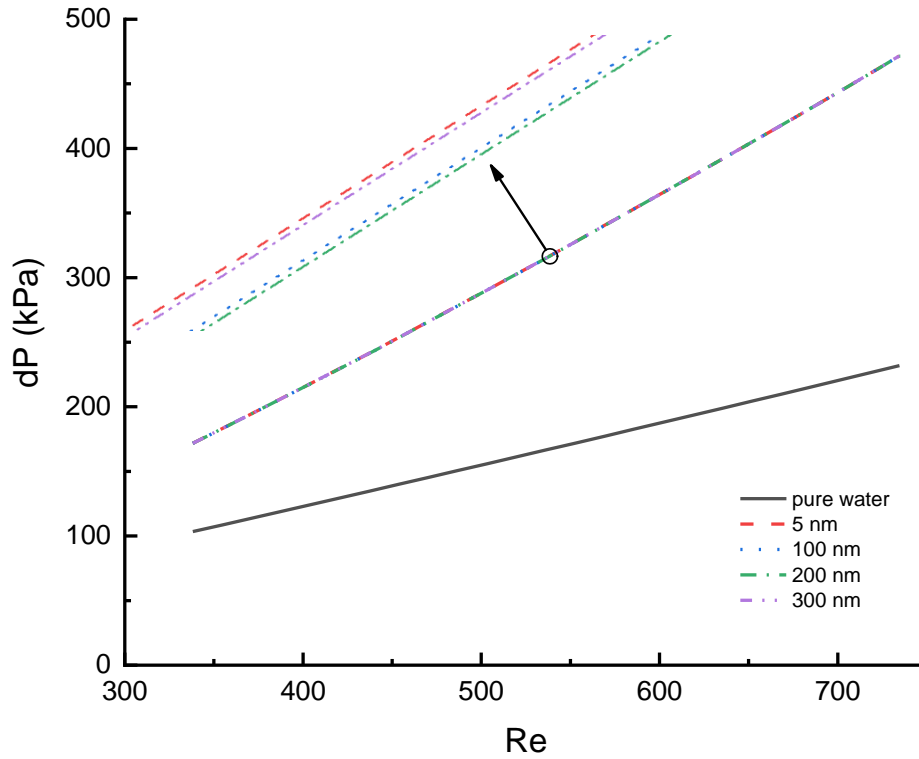
selecting proper *Re* might have a better effect on reducing energy consumption during operation. It is also suggested that lowering fluid flow velocity inside MCHS might have a dual effect in enhancing the performance of MCHS in terms of lowering both pressure drop and thermal resistance. However, it is noticed that adding additional Boron Nitride Nanotube (BNNT) and Triton TX-100 surfactant increases the pressure drop slightly. In turn, this will cause more pumping power required for these substances. The reason is that these additional substances increase fluid viscosity. As seen in Eq. (23), the fluid velocity directly depends on fluid viscosity. Increasing fluid viscous will impede the fluid motion, thus resulting in more pressure drop as indicated in Eq. (22), in which velocity is inversely proportional to pressure drop. Since the additional nanotube and surfactant will cause a pressure drop, further investigation is required to understand whether different concentrations can minimize the pressure drop. Figure 12a demonstrates pressure drop against *Re* with different volume fractions of the surfactant. As anticipated, adding more volume fraction of the surfactant in the nanofluid will increase the pressure drop. This is because the base fluid receives more fluid density and viscosity. In turn, this will increase the pressure drop, as explained before, so more pumping power is required to move the fluid. However, the selection of volume fraction should be considered as adding less surfactant may provide an advantage in minimizing pressure drop but also destabilize the nanotube. That would affect the increase of thermal resistance, as explained in Figure 8a. However, the trend for Figure 13b and Figure 13c seem insignificant for varying the mass fraction and the nanotube size. However, additional surfactant and nanotubes have increased pressure drop by 75 % at *Re* of 350 and 125% at *Re* of 700.

(a)

(b)

500

400

dP (kPa)

300

200

100

0

300   400   500   600   700

Re

pure water
5 nm
100 nm
200 nm
300 nm

(c)

Figure 13. Effects of pressure drop on Reynold number with different of (a) TX-100 surfactant volume fraction, (b) BNNT nanoparticle mass fraction, and (c) size of nanoparticle diameter

Conclusion

In the present study, a numerical CFD approach was adopted to explore the two objectives: flow pattern and heat transfer performance of microchannel heat sink using Boron Nitride nanotube (BNNT) with the surfactant, Triton X-100. Significant findings following the two objectives revealed that surfactant TX-100 inside nanofluid reduced the fully-develop-flow length compared with pure water alone. The pure water took more time to achieve a fully developed flow inside the microchannel heat sink cavity. The thermal resistance drops as much

as 90 % compared to pure water with a surfactant concentration of 0.35 *vol.* % and adding 0.02 *wt.* % especially at a low Reynold number (*Re*) of 400. It was discovered that the Nusselt number (*Nu*) increased twice from the pure water with additional 0.35 *vol.* % of surfactant after *Re* of 400. The biggest nanotube size has increased the Nu with the Re. However, improving the thermal performance with additional surfactant and nanotubes, the pressure drop seems to be a drawback factor for the nanofluid with surfactant implementation in the microchannel. However, additional surfactant and nanotubes have increased pressure drop by 75 % at *Re* of 350 and 125% at *Re* of 700.

References

Alfaryjat, A., Mohammed, H., Adam, N. M., Stanciu, D., & Dobrovicescu, A. (2018). Numerical investigation of heat transfer enhancement using various nanofluids in hexagonal microchannel heat sink. *Thermal Science and Engineering Progress, 5*, 252-262.

Alhamid, M., Nasruddin, N., Susanto, E., Vickary, T., & Budiyanto, M. (2019). Refrigeration cycle exergy-based analysis of hydrocarbon (r600a) refrigerant for optimization of household refrigerator. *Evergreen, 6*(1), 71-77.

Ardiansyah, S. R., Orlando, A. M., Rahman, A., & Prihantini, N. B. (2019). Tubular photobioreactor: A preliminary experiment using synechococcus sp.(cyanobacteria) cultivated in NPK media for biomass production as biofuel feedstock. *Evergreen, 6*(2), 157-161.

Babu, J. R., Kumar, K. K., & Rao, S. S. (2017). State-of-art review on hybrid nanofluids. *Renewable and Sustainable Energy Reviews, 77*, 551-565.

Bahiraei, M., Heshmatian, S., Goodarzi, M., & Moayedi, H. (2019). CFD analysis of employing a novel ecofriendly nanofluid in a miniature pin fin heat sink for cooling of electronic components: Effect of different configurations. *Advanced Powder Technology, 30*(11), 2503-2516.

Bahiraei, M., Mazaheri, N., & Daneshyar, M. R. (2021). Employing elliptical pin-fins and nanofluid within a heat sink for cooling of electronic chips regarding energy efficiency perspective. *Applied thermal engineering, 183*, 116159.

Bahiraei, M., & Monavari, A. (2020). Impact of nanoparticle shape on thermohydraulic performance of a nanofluid in an enhanced microchannel heat sink for utilization in cooling of electronic components. *Chinese Journal of Chemical Engineering*.

Choi, T. J., Jang, S. P., & Kedzierski, M. (2018). Effect of surfactants on the stability and solar thermal absorption characteristics of water-based nanofluids with multi-walled carbon nanotubes. *International Journal of Heat and Mass Transfer, 122*, 483-490.

Chuan, L., Wang, X.-D., Wang, T.-H., & Yan, W.-M. (2015). Fluid flow and heat transfer in microchannel heat sink based on porous fin design concept. *International Communications in Heat and Mass Transfer, 65*, 52-57.

Dey, D., Kumar, P., & Samantaray, S. (2017). A review of nanofluid preparation, stability, and thermo-physical properties. *Heat Transfer—Asian Research, 46*(8), 1413-1442.

Drummond, K. P., Back, D., Sinanis, M. D., Janes, D. B., Peroulis, D., Weibel, J. A., & Garimella, S. V. (2018). A hierarchical manifold microchannel heat sink array for high-heat-flux two-phase cooling of electronics. *International journal of heat and mass transfer, 117*, 319-330.

Ealia, S. A. M., & Saravanakumar, M. (2017). *A review on the classification, characterization, synthesis of nanoparticles and their application.* Paper presented at the IOP Conference Series: Materials Science and Engineering.

Esfe, M. H., Nadooshan, A. A., Arshi, A., & Alirezaie, A. (2018). Convective heat transfer and pressure drop of aqua based TiO2 nanofluids at different diameters of nanoparticles: data analysis and modeling with artificial neural network. *Physica E: Low-dimensional Systems and Nanostructures, 97*, 155-161.

Fisher, T. S., & Torrance, K. E. (2001). Optimal shapes of fully embedded channels for conjugate cooling. *IEEE Transactions on advanced packaging, 24*(4), 555-562.

Ghani, I. A., Sidik, N. A. C., Mamat, R., Najafi, G., Ken, T. L., Asako, Y., & Japar, W. M. A. A. (2017). Heat transfer enhancement in microchannel heat sink using hybrid technique of ribs and secondary channels. *International journal of heat and mass transfer, 114*, 640-655.

Ghasemi, B., & Aminossadati, S. (2010). Brownian motion of nanoparticles in a triangular enclosure with natural convection. *International journal of thermal sciences, 49*(6), 931-940.

Ghorabaee, H., Emami, M. R. S., & Shafahi, M. (2020). Effect of nanofluid and surfactant on thermosyphon heat pipe performance. *Heat transfer engineering, 41*(21), 1829-1842.

Gómez-Villarejo, R., Aguilar, T., Hamze, S., Estellé, P., & Navas, J. (2019). Experimental analysis of water-based nanofluids using boron nitride nanotubes with improved thermal properties. *Journal of Molecular Liquids, 277*, 93-103.

Gong, L., Li, Y., Bai, Z., & Xu, M. (2018). Thermal performance of micro-channel heat sink with metallic porous/solid compound fin design. *Applied thermal engineering, 137*, 288-295.

Halelfadl, S., Adham, A. M., Mohd-Ghazali, N., Maré, T., Estellé, P., & Ahmad, R. (2014). Optimization of thermal performances and pressure drop of rectangular microchannel heat sink using aqueous carbon nanotubes based nanofluid. *Applied thermal engineering, 62*(2), 492-499.

Heidarshenas, A., Azizi, Z., Peyghambarzadeh, S., & Sayyahi, S. (2021). Experimental investigation of heat transfer enhancement using ionic liquid-Al2O3 hybrid nanofluid in a cylindrical microchannel heat sink. *Applied thermal engineering, 191*, 116879.

Hong, F., Cheng, P., Ge, H., & Joo, G. T. (2007). Conjugate heat transfer in fractal-shaped microchannel network heat sink for integrated microelectronic cooling application. *International journal of heat and mass transfer, 50*(25-26), 4986-4998.

Husain, A., & Kim, K.-Y. (2008). Optimization of a microchannel heat sink with temperature dependent fluid properties. *Applied thermal engineering, 28*(8-9), 1101-1107.

Japar, W. M. A. A., Sidik, N. A. C., & Mat, S. (2018). A comprehensive study on heat transfer enhancement in microchannel heat sink with secondary channel. *International Communications in Heat and Mass Transfer, 99*, 62-81.

Jebasingh, B. E., & Arasu, A. V. (2020). A comprehensive review on latent heat and thermal conductivity of nanoparticle dispersed phase change material for low-temperature applications. *Energy Storage Materials, 24*, 52-74.

Khairul, M., Shah, K., Doroodchi, E., Azizian, R., & Moghtaderi, B. (2016). Effects of surfactant on stability and thermo-physical properties of metal oxide nanofluids. *International journal of heat and mass transfer, 98*, 778-787.

Kiliç, F., Menlik, T., & Sözen, A. (2018). Effect of titanium dioxide/water nanofluid use on thermal performance of the flat plate solar collector. *Solar Energy, 164*, 101-108.

Knight, R. W., Hall, D. J., Goodling, J. S., & Jaeger, R. C. (1992). Heat sink optimization with application to microchannels. *IEEE Transactions on Components, Hybrids, and Manufacturing Technology, 15*(5), 832-842.

Lee, J., & Mudawar, I. (2007). Assessment of the effectiveness of nanofluids for single-phase and two-phase heat transfer in micro-channels. *International journal of heat and mass transfer, 50*(3-4), 452-463.

Leng, C., Wang, X.-D., Wang, T.-H., & Yan, W.-M. (2015). Optimization of thermal resistance and bottom wall temperature uniformity for double-layered microchannel heat sink. *Energy Conversion and Management, 93*, 141-150.

Li, X., Zhu, D., Wang, X., Wang, N., Gao, J., & Li, H. (2008). Thermal conductivity enhancement dependent pH and chemical surfactant for Cu-H2O nanofluids. *Thermochimica Acta, 469*(1-2), 98-103.

Mat, M. N. H., Asmuin, N. Z., Basir, M. F. M., Abbas, T., Kasihmuddin, M. S. M., & Goodarzi, M. (2021). Influence of nozzle area ratio on the gas-particle flow for single-hose dry ice blasting nozzle. *Journal of thermal analysis and calorimetry, 143*(3), 2343-2354.

Mat, M. N. H., Asmuin, N. Z., Basir, M. F. M., Goodarzi, M., Abd Rahman, M. F., Khairulfuaad, R., . . . Kasihmuddin, M. S. M. (2020). Influence of divergent length on the gas-particle flow in dual hose dry ice blasting nozzle geometry. *Powder Technology, 364*, 152-158.

Mat, M. N. H., Asmuin, N. Z., Basir, M. F. M., Safaei, M. R., Kasihmuddin, M. S. M., Khairuddin, T. K. A., & Godarzi, M. (2021). Optimizing nozzle convergent angle using central composite design on the particle velocity and acoustic power level for single-hose dry ice blasting nozzle. *Journal of thermal analysis and calorimetry, 144*(6), 2159-2173.

Monavari, A., Jamaati, J., & Bahiraei, M. (2021). Thermohydraulic performance of a nanofluid in a microchannel heat sink: Use of different microchannels for change in process intensity. *Journal of the Taiwan Institute of Chemical Engineers, 125*, 1-14.

Murshed, S., Leong, K., & Yang, C. (2005). Enhanced thermal conductivity of TiO2—water based nanofluids. *International journal of thermal sciences, 44*(4), 367-373.

Roache, P. J., & Knupp, P. M. (1993). Completed richardson extrapolation. *Communications in Numerical Methods in Engineering, 9*(5), 365-374.

Shamsuddin, H. S., Estellé, P., Navas, J., Mohd-Ghazali, N., & Mohamad, M. (2021). Effects of surfactant and nanofluid on the performance and optimization of a microchannel heat sink. *International Journal of Heat and Mass Transfer, 175*, 121336.

Shen, H., Jin, X., Zhang, F., Xie, G., Sunden, B., & Yan, H. (2017). Computational optimization of counter-flow double-layered microchannel heat sinks subjected to thermal resistance and pumping power. *Applied thermal engineering, 121*, 180-189.

Singh, J., Rudman, M., & Blackburn, H. (2017). The effect of yield stress on pipe flow turbulence for generalized Newtonian fluids. *Journal of Non-Newtonian Fluid Mechanics, 249*, 53-62.

Taylor, M. A. (2011). Conservation of mass and energy for the moist atmospheric primitive equations on unstructured grids. In *Numerical techniques for global atmospheric models* (pp. 357-380): Springer.

Tuckerman, D. B., & Pease, R. F. W. (1981). High-performance heat sinking for VLSI. *IEEE Electron device letters, 2*(5), 126-129.

Wei, X., & Joshi, Y. (2003). Optimization study of stacked micro-channel heat sinks for micro-electronic cooling. *IEEE transactions on components and packaging technologies, 26*(1), 55-61.

Weisberg, A., Bau, H. H., & Zemel, J. (1992). Analysis of microchannels for integrated cooling. *International journal of heat and mass transfer, 35*(10), 2465-2474.

Xia, G., Ma, D., Zhai, Y., Li, Y., Liu, R., & Du, M. (2015). Experimental and numerical study of fluid flow and heat transfer characteristics in microchannel heat sink with complex structure. *Energy Conversion and Management, 105*, 848-857.

Yu, W., Xie, H., Chen, L., & Li, Y. (2010). Investigation on the thermal transport properties of ethylene glycol-based nanofluids containing copper nanoparticles. *Powder Technology, 197*(3), 218-221.

Zhou, J., Cao, X., Zhang, N., Yuan, Y., Zhao, X., & Hardy, D. (2020). Micro-channel heat sink: a review. *Journal of Thermal Science, 29*(6), 1431-1462.